Published in final edited form as:
J Biomech. 2013 February 22; 46(4): 723–730. doi:10.1016/j.jbiomech.2012.11.039.

Bone Fragility Beyond Strength and Mineral Density: Raman Spectroscopy Predicts Femoral Fracture Toughness in a Murine Model of Rheumatoid Arthritis

Jason A. Inzana[1,2], **Jason R. Maher**[3], **Masahiko Takahata**[2], **Edward M. Schwarz**[2], **Andrew J. Berger**[3], and **Hani A. Awad**[1,2]

[1]Department of Biomedical Engineering, 207 Robert B. Goergen Hall, University of Rochester, Rochester, NY

[2]The Center for Musculoskeletal Research, 601 Elmwood Avenue, University of Rochester Medical Center, Rochester, NY

[3]The Institute of Optics, 275 Hutchinson Road, University of Rochester, Rochester, NY

Abstract

Clinical prediction of bone fracture risk primarily relies on measures of bone mineral density (BMD). BMD is strongly correlated with bone strength, but strength is independent of fracture toughness, which refers to the bone's resistance to crack initiation and propagation. In that sense, fracture toughness is more relevant to assessing fragility-related fracture risk, independent of trauma. We hypothesized that bone biochemistry, determined by Raman spectroscopy, predicts bone fracture toughness better than BMD. This hypothesis was tested in tumor necrosis factor-transgenic mice (TNF-tg), which develop inflammatory-erosive arthritis and osteoporosis. The left femurs of TNF-tg and wild type (WT) littermates were measured with Raman spectroscopy and micro-computed tomography. Fracture toughness was assessed by cutting a sharp notch into the anterior surface of the femoral mid-diaphysis and propagating the crack under 3 point bending. Femoral fracture toughness of TNF-tg mice was significantly reduced compared to WT controls (p=0.04). A Raman spectrum-based prediction model of fracture toughness was generated by partial least squares regression (PLSR). Raman spectrum PLSR analysis produced strong predictions of fracture toughness, while BMD was not significantly correlated and produced very weak predictions. Raman spectral components associated with mineralization quality and bone collagen were strongly leveraged in predicting fracture toughness, reiterating the limitations of mineralization density alone.

Keywords

Fracture Toughness; Raman Spectroscopy; Bone Mineral Density; Bone Quality; Inflammatory Arthritis

Corresponding Author. Hani A. Awad, PhD, Department of Biomedical Engineering, The Center for Musculoskeletal Research, University of Rochester Medical Center – Box 665, 601 Elmwood Avenue, Rochester, NY 14642, (585) 273-5268, Hani_Awad@URMC.Rochester.edu.

Disclosure

The authors have no conflicts of interest and nothing to disclose.

1. Introduction

Bone fragility fractures that occur in the absence of significant trauma are often associated with primary or secondary osteoporosis, and can result in serious patient morbidity and mortality (Johnell et al., 2004). Therefore, it is necessary to accurately identify high risk patients who require intervention, without imposing the unnecessary costs that could result from false positive classifications. Currently, individualized prediction of bone fracture risk primarily relies on measures of bone mineral density (BMD), often determined through dual energy X-ray absorptiometry (DXA), as well as clinical risk factors such as smoking, glucocorticoid treatment, and rheumatoid arthritis (RA) (Kanis et al., 2008; van Staa et al., 2006; Van Staa et al., 2003). DXA bone scans provide a T-score for anatomic sites of interest, such as the hip and spine, that describes the patient's deviation in areal BMD from an average young adult of the same gender and ethnicity. For women, the World Health Organization defines osteoporosis as a T-score below −2.5 (Kanis et al., 1994; WHO, 1994). When this standard definition of osteoporosis was used to classify female patients at high risk of bone fracture in a sample population, the sensitivity of fracture prediction was only 22.4% (Tremollieres et al., 2010). This evidence underscores the critical need for improved technologies and prediction modalities that will enable more sensitive and specific bone fracture risk predictions.

BMD is controversial as a predictor of fracture risk (Burger et al., 1999; Cranney et al., 2007; Cummings et al., 1993; Cummings et al., 2006; De Laet et al., 1998; Siris et al., 2004; Stone et al., 2003; Van Staa et al., 2003). The complex composition and structure underlying the mechanical integrity of bone likely explains the limitation of DXA bone scans to accurately predict fracture susceptibility. Indeed, ex vivo biomechanical studies have reported significant correlations between BMD and whole bone strength in a variety of loading modalities (Huber et al., 2008; Nielsen et al., 2007; Perilli et al., 2012). However, these strength-based measures do not account for bone's fatigue response or fracture toughness, which are important considerations in defining bone quality and predicting fragility fracture risk. Fracture toughness is generally independent of strength and refers to bone's ability to resist fracture by dissipating high local stresses associated with crack initiation and propagation (Ritchie, 2011). Bone is a complex heterogeneous and anisotropic composite of mineral (primarily calcium phosphate) and organic (primarily collagen) matrix with structural organization spanning multiple size scales. Within lamellar bone, collagen microfibrils are organized in oriented arrays that form the foundational substructure of bone. Hydroxyapatite-like mineral crystals, which are often calcium-deficient and contain carbonate and other substitutions compared to stoichiometric hydroxyapatite, are deposited within and around this collagen matrix (Fratzl et al., 2004; Glimcher, 1984; Landis et al., 1996). The toughness of bone derives from the micro- and nano-structural organization as well as reinforcement to the brittle mineral phase by the underlying collagen matrix. The interested reader is referred to excellent reviews on strength versus fracture toughness (Ritchie, 2011) and the toughness of bone (Launey et al., 2010; Ritchie, 2010; Zimmermann et al., 2012) for more details.

Pathological changes that occur with natural aging and through a variety of disease processes lead to compositional and structural changes in the bone, including loss of mineral mass in osteoporosis (Kanis et al., 1994), non-enzymatic glycation of collagen in type 1 diabetes (Saito and Marumo, 2010; Silva et al., 2009; Tang and Vashishth, 2011; Vashishth, 2007), or concomitant deterioration in the mineral and organic phases of the bone matrix in inflammatory diseases such as RA (Abdulghani et al., 2009; David and Schett, 2010; Lacativa and Farias, 2010; Li and Schwarz, 2003; Romas, 2005; Takahata et al., 2012).

These changes invariably affect bone strength and toughness, which cannot be noninvasively measured or reliably predicted with current clinical technologies.

There is a critical need for improved diagnostic modalities to detect compositional changes in bone and predict the strength-independent functional properties such as fracture toughness. Raman spectroscopy is a promising technology that can produce unique information about the compositional biochemistry of bone by measuring light scattering that results from molecular vibrations, with spectral shifting that corresponds to the unique vibrational energy levels within each type of molecule. Pathological changes in matrix components, including phosphate and carbonate as well as the amide backbone of collagen, can be detected by Raman spectroscopy, but not through currently available clinical tools (Carden and Morris, 2000). Therefore, we hypothesized that Raman spectroscopy would predict pathological changes to cortical bone fracture toughness while BMD alone would not provide accurate predictions. This hypothesis was tested using a transgenic murine model of RA, which constitutively overexpresses the inflammatory cytokine tumor necrosis factor-alpha (TNF-α) and develops secondary osteoporosis.

2. Methods

2.1 Animals and Tissue Processing

All animal studies were performed in accordance with protocols approved by the University of Rochester's Committee on Animal Resources. TNF-transgenic (TNF-tg) mice (line 3647 in a C57BL/6J background) (Keffer et al., 1991) and wild type (WT) C57BL/6J mice were used in this study (n = 7 per group). The TNF-tg mice serve as a model of RA and invariably develop chronic inflammation and erosive arthritis with secondary osteoporosis by five months of age (Proulx et al., 2007; Takahata et al., 2012). The left femurs of male mice from each genotype in the age range of 20–22 weeks were collected for imaging and biomechanical testing. Each bone was cleaned and stored at −80°C until the day of micro-computed tomography (micro-CT) and Raman spectroscopic measurements, as well as subsequent biomechanical testing.

2.2 Micro-Computed Tomography

The left femur of each mouse was scanned by micro-CT (VivaCT 40; Scanco Medical; Bassersdorf, Switzerland), at a 10.5-micron isotropic resolution using an integration time of 300 ms, energy of 55 kVp, and intensity of 145 μA. The cortical bone mineral density (BMD), cortical thickness, and area moment of inertia about the major cross-sectional axis were measured by averaging over a region of 300 microns (28 slices) at the femoral mid-shaft.

2.3 Raman Spectroscopy

Following micro-CT, Raman spectra were acquired from the medial mid-diaphysis of the same femurs over a 3.5 mm^2 area using a locally constructed Raman spectroscopy system (Maher et al., 2011). All spectra were truncated to the 910–1740 cm^{-1} region, which includes many relevant mineral and organic matrix bands (Carden and Morris, 2000), and normalized to their mean absolute deviations. Commonly studied component ratios were calculated, such as the phosphate mineral-to-matrix ratio (PMMR) based on the phosphate ν_1 (924–986 cm^{-1}) and amide I (1596–1730 cm^{-1}) areas, phosphate-to-carbonate ratio (PCR) based on the phosphate ν_1 and carbonate ν_1 (1057–1098 cm^{-1}) areas, carbonate mineral-to-matrix ratio (CMMR), and the amide I 1660 cm^{-1}/1690 cm^{-1} ratio. Peak areas were calculated by summing the Raman intensity in the spectral regions listed above. The full width half maximal (FWHM) bandwidth of the phosphate ν_1 peak, which is related to

mineral crystallinity (Morris and Mandair, 2011; Penel et al., 1998), was calculated by fitting with a single Gaussian curve.

2.4 Femoral Fracture Toughness

Fracture toughness of the same femoral mid-diaphysis was subsequently measured by methods adapted from Ritchie et al. (Ritchie et al., 2008). Specifically, a razor sharp circumferential through-wall notch was cut into the anterior surface of the femoral diaphysis. A starter notch was cut with a 0.22 mm gigli saw (RISystem; Davos, Switzerland), which was then sharpened using a razor blade under irrigation with a 1 μm diamond suspension. The notches were cut to relative depths to produce half-notch angles of 75° ± 4.1° (Fig. 1*h*). The anterior surface was chosen for notching based on findings suggesting that physiological loading is primarily tensile in the anterior quadrant of rat and mouse femora (Indrekvam et al., 1991; Ramasamy and Akkus, 2007; Vashishth, 2008). After notching, the bones were stored in PBS overnight at 4°C and then allowed to warm to room temperature prior to three-point bending, which was conducted using an Instron 8841 DynaMight™ Axial Testing System (Instron Corp.; Canton, MA) with a 6 mm support span and a 50 N load cell. Bending tests were performed at a displacement rate of 0.001 mm/s until failure (fast fracture) with the femurs submerged in PBS and the anterior, notched side of the bone in tension. A stereomicroscope was used to ensure that the loading post was aligned precisely in plane with the notch (Fig. 1*a,b*).

After testing, bone specimens were fixed, dehydrated, and gold sputter coated for scanning electron micrograph (SEM; LEO 982 FE-SEM; Carl Zeiss SMT; Thornwood, NY) imaging to assess the extent of sub-critical (stable) crack growth prior to fracture. The half-crack angle, average cortical thickness, and mean radii were measured from backscattered SEM images of the fracture surfaces using custom algorithms written in MATLAB (R2011a; MathWorks Inc.; Natick, MA). Micro-CT based measures of mean cortical thickness around the full bone circumference were not used because the anterior quadrant, once notched, does not contribute to the load response during testing and is generally thicker, which would bias the measurements. These data along with the fracture load and support span were used to estimate the critical stress intensity factor (K_C; fracture toughness) for each specimen (Ritchie et al., 2008) according to:

$$K_C = F_b \frac{P_f S R_o}{\pi(R_o^4 - R_i^4)} \sqrt{\pi R_m \theta_C}$$

where P_f is the load at fracture, S is the span length, R_o and R_i are the mean outer and inner radii, R_m is the average of R_o and R_i, θ_C is the half-crack angle at fracture instability, and F_b is a geometry factor for a thick-walled pipe as defined by Takahashi (Takahashi, 2002).

2.6 Statistics

All comparisons between WT and TNF-tg mice were made using an unpaired t-test, with Welch's correction for heteroscedastic data. A predictive model of the measured fracture toughness was generated from the full Raman spectrum (910 cm^{-1}–1740 cm^{-1}) of each bone using partial-least squares regression (PLSR), as we have described previously with whole bone torsional strength (Maher et al., 2011). Two PLSR components were chosen to fit the model based on minimization of the root mean squared error of cross-validation (RMSECV) and a significant reduction in RMSECV from a single component according to an F-test. Correlations of the measured fracture toughness with individual metrics, such as BMD and Raman peak area ratios, were assessed through univariate linear regression. All fracture toughness predictions were calculated using a leave-one-out cross-validation (LOOCV)

technique. Finally, a stepwise multilinear regression of the fracture toughness on all of the calculated Raman metrics was performed to determine which metrics significantly contribute to a multiple regression model. Statistical significance was accepted for $p < 0.05$ in all analyses.

3. Results

3.1 Femoral Fracture Toughness

Consistent with previous data (Takahata et al., 2012), the TNF-tg mice had significantly reduced cortical thickness, mean radii, and area moment of inertia about the cross-sectional major axis compared to WT (Fig. 1*c–e*). Stable crack extension was similar between the groups, which initiated from consistent notch depths (Fig. 1*f,g*). The deterioration in structure and bone quality of TNF-tg mice relative to WT were manifest in significantly lower fracture loads (4.31±0.90 vs. 6.04±1.18 N; $p<0.01$) and bending stiffness (52.3±7.5 vs. 62.6±9.1 N/mm; $p<0.05$) during notched 3-point bending (Fig. 2*a*). Fracture toughness of femoral cortical bone in TNF-tg mice was significantly reduced compared to WT controls (Fig. 2*b*). However, both genotypes showed qualitatively similar stable crack propagation prior to fracture instability (Fig. 2*c,d*).

3.2 Comparisons of Femoral Composition

Cortical BMD measured by micro-CT at the mid-diaphysis was not significantly different between the TNF-tg and WT mice (Fig. 3*a*). Raman spectroscopy metrics, including the PMMR and PCR were significantly higher in TNF-tg mice (Fig. 3*b,c*). The amide I ratio and the CMMR were not significantly changed in TNF-Tg compared to WT (Fig. 3*d,e*). Mineral crystallinity (defined as the phosphate ν_1 $FWHM^{-1}$; (Morris and Mandair, 2011; Penel et al., 1998)) was also not significantly different between the two genotypes.

3.3 Prediction of Femoral Fracture Toughness

PLSR analysis of the full Raman spectrum resulted in a strong prediction model of the femoral fracture toughness, with a root mean squared error of cross-validation (RMSECV) of 0.25 MPa $\sqrt{m}$ (Fig. 4). In contrast, BMD was not significantly correlated with, nor was able to accurately predict the measured bone fracture toughness (Fig. 4). Multiple individual metrics derived from the Raman spectra were significantly correlated with bone fracture toughness (Table 1). Both PMMR and mineral crystallinity were strongly (negatively) correlated with fracture toughness (R^2=0.7 and 0.6, respectively, $p<0.05$). Step-wise multilinear regression of fracture toughness on all of the calculated Raman metrics included only the PMMR and mineral crystallinity in the final model (R^2=0.83, $p<0.05$; Table 1).

To explore the relative contributions from each predictive variable (Raman intensity at each wavenumber) to the final model, we analyzed the loadings for each of the two PLSR components. The Variable Importance in Projection (VIP) Score is used to assess the contribution of each variable to the final predictions, with scores ≥ 1 generally set as the cut-off for importance (Chong and Jun, 2005; Wold et al., 1993). Examining the PLSR component loadings of wavenumbers with VIP scores ≥ 1 reveals leveraging by aspects of the phosphate ν_1 peak as well as organic matrix components (amides I, II, and III and CH_2). The carbonate ν_1 peak and hydrogen phosphate peak (HPO_4^{2-}; 1000–1006 cm^{-1}) also contribute to the predictive component loadings (Fig. 5). Plotting the Raman spectra as a function of measured fracture toughness qualitatively reiterates the differentials provided by the quantitative regression analyses described above (Fig. 6).

4. Discussion

While it is well accepted that BMD is strongly correlated with bone strength, our data suggest that BMD is not well correlated with cortical bone fracture toughness, especially when the underlying pathology does not elicit profound changes in BMD. In contrast, Raman-based mineral metrics, such as the crystallinity and PMMR, were significantly correlated with fracture toughness. Detecting these subtle changes in mineral and organic matrix quality within bones having subtle or no difference in BMD is important in discriminating bones with varying fracture toughness.

Bone mineral is composed of poorly crystallized, calcium deficient apatite containing hydrogen phosphate (HPO_4^{2-}), carbonate (CO_3^{2-}) and other ions (Farlay et al., 2010). Carbonate for phosphate ion substitution has the effect of decreasing crystallite size and increasing the number of vacancies or defects with the apatite lattice (Porter et al., 2005). In mature bone, the presence of numerous defects in the stable, non-stoichiometric apatite crystals (Farlay et al., 2010) might have negative effects on bone mineral quality. The effect of sustained TNF-α overexpression on carbonate substitution appears to be minimal in our study as evidenced by the negligible variations in the carbonate peak (1070 cm^{-1}; Fig. 6*c*). However, there was variation in the monohydrogen phosphate peak (HPO_4^{2-}; 1000–1006 cm^{-1}; Fig. 6*b*) and the spectral location of the phosphate ν_1 peak (Fig. 6*a*). The first component loading indicates substantial negative associations of increasing HPO_4^{2-} with fracture toughness (Fig. 5). The first and second component loadings reach maximal negative peaks at 968 cm^{-1} and 966 cm^{-1}, respectively, suggesting that fracture toughness decreases as the phosphate ν_1 peak shifts towards this spectral region. Studies have found that octacalcium phosphate [OCP; $Ca_8(HPO_4)_2(PO_4)_4{\cdot}5H_2O$], which has been suggested as an apatitic precursor in biomineralization (Brown, 1962; Wang et al., 2008), has a Raman peak in the 966–970 cm^{-1} range (Crane et al., 2006; Fowler et al., 1993; Sauer et al., 1994). Supporting this hypothesis, a direct correlation was observed between the OCP area (966–970 cm^{-1}) and the HPO_4^{2-} area (1000–1006 cm^{-1}) in this study (R^2=0.65, p<0.001). This is consistent with reports that found the HPO_4^{2-} peak at 1003 cm^{-1} to be strongly associated with regions of new trabecular bone formation through factor analysis of Raman spectra (Timlin et al., 1999).

While alterations in the mineral components account for significant variance in the whole bone fracture toughness, correlations become stronger when components of the collagen phase are considered. Specifically, the amide I, II, and III regions of the Raman spectrum as well as the CH_2 region provide additional contributions to the PLSR component loadings (Fig. 5). Increases in the amide I (Fig. 6*g*) and CH_2 (Fig. 6*e*) signals and a decrease in the amide II signal (Fig. 6*f*) were directly associated with increased fracture toughness. However, the contributions from the amide III region (Fig. 6*d*) were more complex as it was leveraged in both PLSR components, but in opposing directions (Fig. 5). In contrast to our findings, Ritchie et al. demonstrated profound increases with aging in the amide I peaks of deep UV-Raman spectra, which were correlated with aging-related deterioration in crack-initiation toughness (Ritchie et al., 2006). However, Ritchie et al. used human cortical bone with crack extension in the longitudinal direction of the bone shaft, while we studied transverse crack extension through murine bone. This could explain the disparity in our findings, considering that collagen fibril matrix is preferentially oriented in plane with the bone axis. Further, the effects of physiological changes to collagen, such as side chain variations or cross-linking, on the Raman amide I band are not well understood. While mechanistic differences in toughness deterioration may exist between inflammatory diseases and natural aging, there is a clear role of collagen in fracture toughness and bone quality.

Multiple studies have examined correlations between bone mechanical properties and Raman spectroscopy-based measures of bone composition (Akkus et al., 2004; Bi et al., 2011; Maher et al., 2011; Raghavan et al., 2012; Ramasamy and Akkus, 2007). Maher et al. found that predictions of tibial torsional strength, generated by a PLSR analysis of the full Raman spectrum, were superior to predictions from the micro-CT structural and BMD parameters (Maher et al., 2011). Others have also found significant correlations of Raman measurements, including mineral-to-matrix ratio, with tissue-scale bone mechanical parameters measured by nano-indentation (Bi et al., 2011; Raghavan et al., 2012). However, relationships between Raman spectroscopic measurements and mechanical properties beyond monotonic strength and stiffness (e.g. plasticity, fatigue, and fracture toughness) are not as well established. Bi et al. found the post-yield deflection of whole murine femurs in 3 point bending was significantly correlated with mineral-to-matrix ratios (negative trend; PO_4^{3-} ν_1/amide I, PO_4^{3-} ν_1/proline, and PO_4^{3-} ν_1/amide III) as well as mineral crystallinity (negative trend) (Bi et al., 2011). Ager et al. found the area ratio of sub-peaks (1610 cm^{-1}/1655 cm^{-1}) in the amide I band, as measured by deep-UV Raman spectroscopy, to be significantly correlated (negative trend) with crack initiation toughness but not crack growth toughness in cortical bone sections from human humeri (Ager et al., 2005). Yerramshetty et al. demonstrated that mineral crystallinity negatively correlates with modulus degradation and positively correlates with cycles to failure in tensile fatigue tests of human femoral cortical bone (Yerramshetty and Akkus, 2008). Our current study adds important information to this field and demonstrates that increases in PMMR, CMMR, and crystallinity as well as shifting of the phosphate ν_1 peak towards 966 cm^{-1} negatively correlate with murine cortical bone fracture toughness. These findings reiterate the mutual exclusivity of strength and toughness and align with the widely accepted functional roles of mineral and collagen in bone: the brittle mineral phase primarily contributes to elastic strength and stiffness while the ductile collagen matrix enhances the plasticity and toughness of bone.

The fracture toughness equation used in this study was derived for cylindrical pipes of uniform wall thickness. Therefore, these calculations have geometry-related assumptions that are violated when applied to murine femurs, as detailed previously (Ritchie et al., 2008). Typically violated assumptions include deviations from circularity and cortical thickness uniformity as well as cortices that are too thin for plane-strain conditions. Ritchie et al. performed a worse-case propagation of errors for the use of this cylindrical tube fracture toughness equation with mouse femurs, and found that the deviation from circularity and non-uniformity of the cortical wall thickness result in 17% uncertainty in the calculated toughness (Ritchie et al., 2008). Considering these potential sources of error, the calculated fracture toughness is unlikely to represent a pure material property for mouse femurs. However, the variation in fracture toughness due to geometrical differences within our dataset was not statistically significant between WT and TNF-tg mice. Therefore, relative comparisons between genotypes and analysis of both genotypes together remain valid.

Raman and Fourier transform infrared (FTIR) spectroscopy have shown the ability to discriminate between patients who experienced a fragility fracture and those who did not. Using Raman, McCreadie et al. found the carbonate/amide I ratio (measured from the femoral head) and the carbonate/phosphate ratio (measured from the iliac crest) were higher in patients who experienced a fragility fracture (McCreadie et al., 2006). Gourion-Arsiquaud et al. found, through FTIR measurements of iliac crest biopsies, that increases in the phosphate/amide I ratio and collagen cross-link ratio in the cortical bone added significantly to correlations with fracture incidence in a multiple logistic regression after including hip BMD (Gourion-Arsiquaud et al., 2009). With continued advances in this technology, Raman spectroscopy could become an important future diagnostic tool for improving patient-specific projections of bone fragility and atypical fracture risk. Further, improved

understanding of patient-specific bone quality deterioration, which Raman spectroscopy may provide, could help guide interventional choices.

Acknowledgments

The Authors would like to thank Mr. Michael Thullen and Ms. Karen Bentley for their excellent technical assistance with micro-CT and SEM imaging, respectively. Jason Inzana is a NSF graduate research fellow (2012116002). The study was supported by pilot funding from the University of Rochester Provost Multidisciplinary Awards as well as grants R21AR061285 and P30AR061307 from NIAMS/NIH. The content is solely the responsibility of the authors and does not necessarily represent the official views of the National Science Foundation, National Institute of General Medical Sciences, or NIH.

References

Abdulghani S, Caetano-Lopes J, Canhao H, Fonseca JE. Biomechanical effects of inflammatory diseases on bone-rheumatoid arthritis as a paradigm. Autoimmun Rev. 2009; 8:668–671. [PubMed: 19223022]

Ager JW, Nalla RK, Breeden KL, Ritchie RO. Deep-ultraviolet Raman spectroscopy study of the effect of aging on human cortical bone. J Biomed Opt. 2005; 10 034012.

Akkus O, Adar F, Schaffler MB. Age-related changes in physicochemical properties of mineral crystals are related to impaired mechanical function of cortical bone. Bone. 2004; 34:443–453. [PubMed: 15003792]

Bi XH, Patil CA, Lynch CC, Pharr GM, Mahadevan-Jansen A, Nyman JS. Raman and mechanical properties correlate at whole bone- and tissue-levels in a genetic mouse model. J Biomech. 2011; 44:297–303. [PubMed: 21035119]

Brown WE. Octacalcium Phosphate and Hydroxyapatite. Nature. 1962; 196 1048-&.

Burger H, de Laet CE, Weel AE, Hofman A, Pols HA. Added value of bone mineral density in hip fracture risk scores. Bone. 1999; 25:369–374. [PubMed: 10495142]

Carden A, Morris MD. Application of vibrational spectroscopy to the study of mineralized tissues (review). J Biomed Opt. 2000; 5:259–268. [PubMed: 10958610]

Chong I-G, Jun C-H. Performance of some variable selection methods when multicollinearity is present. Chemometrics and Intelligent Laboratory Systems. 2005; 78:103–112.

Crane NJ, Popescu V, Morris MD, Steenhuis P, Ignelzi MA Jr. Raman spectroscopic evidence for octacalcium phosphate and other transient mineral species deposited during intramembranous mineralization. Bone. 2006; 39:434–442. [PubMed: 16627026]

Cranney A, Jamal SA, Tsang JF, Josse RG, Leslie WD. Low bone mineral density and fracture burden in postmenopausal women. Cmaj. 2007; 177:575–580. [PubMed: 17846439]

Cummings SR, Black DM, Nevitt MC, Browner W, Cauley J, Ensrud K, Genant HK, Palermo L, Scott J, Vogt TM. Bone density at various sites for prediction of hip fractures. The Study of Osteoporotic Fractures Research Group. Lancet. 1993; 341:72–75. [PubMed: 8093403]

Cummings SR, Cawthon PM, Ensrud KE, Cauley JA, Fink HA, Orwoll ES. BMD and risk of hip and nonvertebral fractures in older men: a prospective study and comparison with older women. J Bone Miner Res. 2006; 21:1550–1556. [PubMed: 16995809]

David JP, Schett G. TNF and bone. Curr Dir Autoimmun. 2010; 11:135–144. [PubMed: 20173392]

De Laet CE, Van Hout BA, Burger H, Weel AE, Hofman A, Pols HA. Hip fracture prediction in elderly men and women: validation in the Rotterdam study. J Bone Miner Res. 1998; 13:1587–1593. [PubMed: 9783547]

Farlay D, Panczer G, Rey C, Delmas PD, Boivin G. Mineral maturity and crystallinity index are distinct characteristics of bone mineral. J Bone Miner Metab. 2010; 28:433–445. [PubMed: 20091325]

Fowler BO, Markovic M, Brown WE. Octacalcium Phosphate .3. Infrared and Raman Vibrational-Spectra. Chem Mater. 1993; 5:1417–1423.

Fratzl P, Gupta HS, Paschalis EP, Roschger P. Structure and mechanical quality of the collagen-mineral nano-composite in bone. Journal of Materials Chemistry. 2004; 14:2115–2123.

Glimcher MJ. Recent studies of the mineral phase in bone and its possible linkage to the organic matrix by protein-bound phosphate bonds. Philos Trans R Soc Lond B Biol Sci. 1984; 304:479–508. [PubMed: 6142489]

Gourion-Arsiquaud S, Faibish D, Myers E, Spevak L, Compston J, Hodsman A, Shane E, Recker RR, Boskey ER, Boskey AL. Use of FTIR Spectroscopic Imaging to Identify Parameters Associated With Fragility Fracture. Journal of Bone and Mineral Research. 2009; 24:1565–1571. [PubMed: 19419303]

Huber MB, Carballido-Gamio J, Bauer JS, Baum T, Eckstein F, Lochmuller EM, Majumdar S, Link TM. Proximal femur specimens: automated 3D trabecular bone mineral density analysis at multidetector CT--correlation with biomechanical strength measurement. Radiology. 2008; 247:472–481. [PubMed: 18430879]

Indrekvam K, Husby OS, Gjerdet NR, Engester LB, Langeland N. Age-dependent mechanical properties of rat femur. Measured in vivo and in vitro. Acta Orthop Scand. 1991; 62:248–252. [PubMed: 2042467]

Johnell O, Kanis JA, Oden A, Sernbo I, Redlund-Johnell I, Petterson C, De Laet C, Jonsson B. Mortality after osteoporotic fractures. Osteoporos Int. 2004; 15:38–42. [PubMed: 14593451]

Kanis JA, Burlet N, Cooper C, Delmas PD, Reginster JY, Borgstrom F, Rizzoli R. European guidance for the diagnosis and management of osteoporosis in postmenopausal women. Osteoporos Int. 2008; 19:399–428. [PubMed: 18266020]

Kanis JA, Melton LJ 3rd, Christiansen C, Johnston CC, Khaltaev N. The diagnosis of osteoporosis. J Bone Miner Res. 1994; 9:1137–1141. [PubMed: 7976495]

Keffer J, Probert L, Cazlaris H, Georgopoulos S, Kaslaris E, Kioussis D, Kollias G. Transgenic mice expressing human tumour necrosis factor: a predictive genetic model of arthritis. EMBO J. 1991; 10:4025–4031. [PubMed: 1721867]

Lacativa PG, Farias ML. Osteoporosis and inflammation. Arq Bras Endocrinol Metabol. 2010; 54:123–132. [PubMed: 20485900]

Landis WJ, Hodgens KJ, Song MJ, Arena J, Kiyonaga S, Marko M, Owen C, McEwen BF. Mineralization of collagen may occur on fibril surfaces: evidence from conventional and high-voltage electron microscopy and three-dimensional imaging. J Struct Biol. 1996; 117:24–35. [PubMed: 8776885]

Launey ME, Buehler MJ, Ritchie RO. On the Mechanistic Origins of Toughness in Bone. Annual Review of Materials Research. 2010; 40:25–53.

Li P, Schwarz EM. The TNF-alpha transgenic mouse model of inflammatory arthritis. Springer Semin Immunopathol. 2003; 25:19–33. [PubMed: 12904889]

Maher JR, Takahata M, Awad HA, Berger AJ. Raman spectroscopy detects deterioration in biomechanical properties of bone in a glucocorticoid-treated mouse model of rheumatoid arthritis. J Biomed Opt. 2011; 16 087012.

McCreadie BR, Morris MD, Chen TC, Sudhaker Rao D, Finney WF, Widjaja E, Goldstein SA. Bone tissue compositional differences in women with and without osteoporotic fracture. Bone. 2006; 39:1190–1195. [PubMed: 16901772]

Morris MD, Mandair GS. Raman assessment of bone quality. Clin Orthop Relat Res. 2011; 469:2160–2169. [PubMed: 21116756]

Nielsen DH, McEvoy FJ, Madsen MT, Jensen JB, Svalastoga E. Relationship between bone strength and dual-energy X-ray absorptiometry measurements in pigs. J Anim Sci. 2007; 85:667–672. [PubMed: 17085729]

Penel G, Leroy G, Rey C, Bres E. MicroRaman spectral study of the PO4 and CO3 vibrational modes in synthetic and biological apatites. Calcif Tissue Int. 1998; 63:475–481. [PubMed: 9817941]

Perilli E, Briggs AM, Kantor S, Codrington J, Wark JD, Parkinson IH, Fazzalari NL. Failure strength of human vertebrae: prediction using bone mineral density measured by DXA and bone volume by micro-CT. Bone. 2012; 50:1416–1425. [PubMed: 22430313]

Porter A, Patel N, Brooks R, Best S, Rushton N, Bonfield W. Effect of carbonate substitution on the ultrastructural characteristics of hydroxyapatite implants. J Mater Sci Mater Med. 2005; 16:899–907. [PubMed: 16167098]

Proulx ST, Kwok E, You Z, Papuga MO, Beck CA, Shealy DJ, Ritchlin CT, Awad HA, Boyce BF, Xing L, Schwarz EM. Longitudinal assessment of synovial, lymph node, and bone volumes in inflammatory arthritis in mice by in vivo magnetic resonance imaging and microfocal computed tomography. Arthritis Rheum. 2007; 56:4024–4037. [PubMed: 18050199]

Raghavan M, Sahar ND, Kohn DH, Morris MD. Age-specific profiles of tissue-level composition and mechanical properties in murine cortical bone. Bone. 2012; 50:942–953. [PubMed: 22285889]

Ramasamy JG, Akkus O. Local variations in the micromechanical properties of mouse femur: the involvement of collagen fiber orientation and mineralization. J Biomech. 2007; 40:910–918. [PubMed: 16678186]

Ritchie RO. How does human bone resist fracture? Ann N Y Acad Sci. 2010; 1192:72–80. [PubMed: 20392220]

Ritchie RO. The conflicts between strength and toughness. Nat Mater. 2011; 10:817–822. [PubMed: 22020005]

Ritchie RO, Koester KJ, Ionova S, Yao W, Lane NE, Ager JW. Measurement of the toughness of bone: A tutorial with special reference to small animal studies. Bone. 2008; 43:798–812. [PubMed: 18647665]

Ritchie RO, Nalla RK, Kruzic JJ, Ager JW, Balooch G, Kinney JH. Fracture and ageing in bone: Toughness and structural characterization. Strain. 2006; 42:225–232.

Romas E. Bone loss in inflammatory arthritis: mechanisms and therapeutic approaches with bisphosphonates. Best Pract Res Clin Rheumatol. 2005; 19:1065–1079. [PubMed: 16301197]

Saito M, Marumo K. Collagen cross-links as a determinant of bone quality: a possible explanation for bone fragility in aging, osteoporosis, and diabetes mellitus. Osteoporosis Int. 2010; 21:195–214.

Sauer GR, Zunic WB, Durig JR, Wuthier RE. Fourier transform Raman spectroscopy of synthetic and biological calcium phosphates. Calcif Tissue Int. 1994; 54:414–420. [PubMed: 8062160]

Silva MJ, Brodt MD, Lynch MA, McKenzie JA, Tanouye KM, Nyman JS, Wang X. Type 1 diabetes in young rats leads to progressive trabecular bone loss, cessation of cortical bone growth, and diminished whole bone strength and fatigue life. J Bone Miner Res. 2009; 24:1618–1627. [PubMed: 19338453]

Siris ES, Chen YT, Abbott TA, Barrett-Connor E, Miller PD, Wehren LE, Berger ML. Bone mineral density thresholds for pharmacological intervention to prevent fractures. Arch Intern Med. 2004; 164:1108–1112. [PubMed: 15159268]

Stone KL, Seeley DG, Lui LY, Cauley JA, Ensrud K, Browner W, Nevitt MC, Cummings SR, Research OF. BMD at multiple sites and risk of fracture of multiple types: Long-term results from the study of osteoporotic fractures. Journal of Bone and Mineral Research. 2003; 18:1947–1954. [PubMed: 14606506]

Takahashi Y. Evaluation of leak-before-break assessment methodology for pipes with a circumferential through-wall crack. Part I: stress intensity factor and limit load solutions. Int J Pres Ves Pip. 2002; 79:385–392.

Takahata M, Maher JR, Juneja SC, Inzana J, Xing L, Schwarz EM, Berger AJ, Awad HA. Mechanisms of bone fragility in a glucocorticoid-treated mouse model of rheumatoid arthritis - implications for insufficiency fracture risk. Arthritis Rheum. 2012

Tang SY, Vashishth D. The relative contributions of non-enzymatic glycation and cortical porosity on the fracture toughness of aging bone. J Biomech. 2011; 44:330–336. [PubMed: 21056419]

Timlin JA, Carden A, Morris MD, Bonadio JF, Hoffler CE, Kozloff KM, Goldstein SA. Spatial distribution of phosphate species in mature and newly generated mammalian bone by hyperspectral Raman imaging. J Biomed Opt. 1999; 4:28–34. [PubMed: 23015166]

Tremollieres FA, Pouilles JM, Drewniak N, Laparra J, Ribot CA, Dargent-Molina P. Fracture risk prediction using BMD and clinical risk factors in early postmenopausal women: sensitivity of the WHO FRAX tool. J Bone Miner Res. 2010; 25:1002–1009. [PubMed: 20200927]

van Staa TP, Geusens P, Bijlsma JW, Leufkens HG, Cooper C. Clinical assessment of the long-term risk of fracture in patients with rheumatoid arthritis. Arthritis Rheum. 2006; 54:3104–3112. [PubMed: 17009229]

Van Staa TP, Laan RF, Barton IP, Cohen S, Reid DM, Cooper C. Bone density threshold and other predictors of vertebral fracture in patients receiving oral glucocorticoid therapy. Arthritis Rheum. 2003; 48:3224–3229. [PubMed: 14613287]

Vashishth D. The role of the collagen matrix in skeletal fragility. Curr Osteoporos Rep. 2007; 5:62–66. [PubMed: 17521507]

Vashishth D. Small animal bone biomechanics. Bone. 2008; 43:794–797. [PubMed: 18672104]

Wang H, Lin CJ, Hu R, Zhang F, Lin LW. A novel nano-micro structured octacalcium phosphate/protein composite coating on titanium by using an electrochemically induced deposition. J Biomed Mater Res A. 2008; 87:698–705. [PubMed: 18200556]

WHO. Assessment of fracture risk and its application to screening for postmenopausal osteoporosis. Report of a WHO Study Group. World Health Organ Tech Rep Ser. 1994; 843:1–129. [PubMed: 7941614]

Wold, S.; Johansson, E.; Cocchi, M. PLS-Partial Least Squares Projections to Latent Structures. In: Kubinyi, H., editor. 3D QSAR in Drug Design, Theory, Methods, and Applications. Leiden: ESCOM Science Publishers; 1993. p. 523-550.

Yerramshetty JS, Akkus O. The associations between mineral crystallinity and the mechanical properties of human cortical bone. Bone. 2008; 42:476–482. [PubMed: 18187375]

Zimmermann EA, Barth HD, Ritchie RO. The Multiscale Origins of Fracture Resistance in Human Bone and Its Biological Degradation. Jom. 2012; 64:486–493.

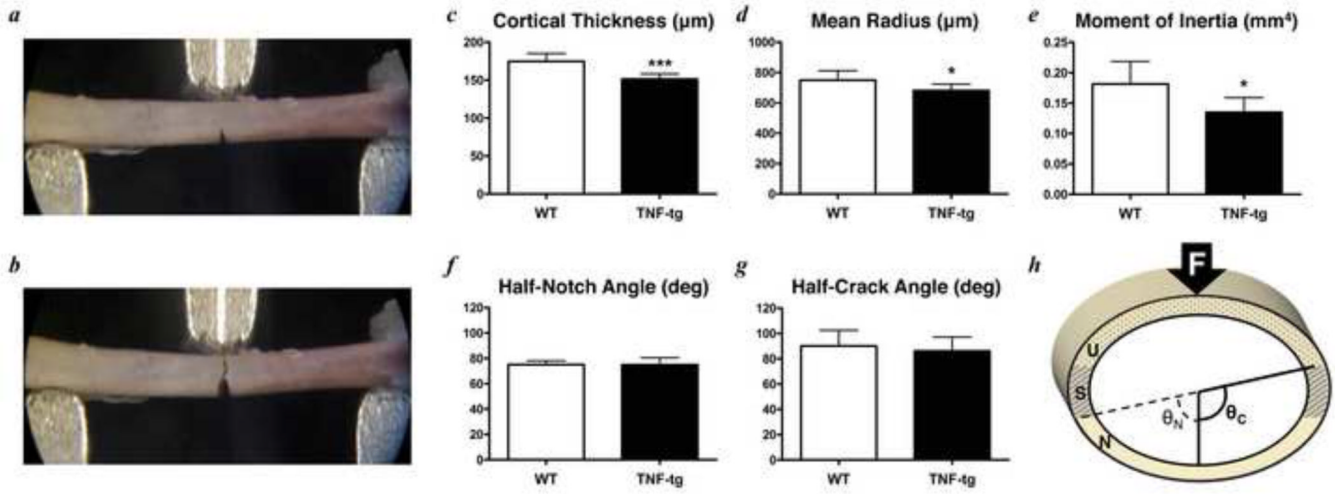

Figure 1. Characterization of the femoral fracture toughness and cross-sections reveals a deteriorated structure in TNF-tg mice, but notch depths are equivalent to WT and crack extension profiles are similar

The notched femur is shown before fracturing (*a*) and after fracturing (*b*) under displacement-controlled 3-point bending. *c*) The average cortical thickness (measured from SEM images) of the non-notched region is significantly greater in the WT mice compared to TNF-tg mice. *d*) The overall mean radius (measured from SEM images) is significantly reduced in TNF-tg mice compared to WT. *e*) The area moment of inertia about the major axis (measured from micro-CT) is significantly reduced in TNF-tg mice, indicating less resistance to bending. *f–g*) The half-notch angle and half-crack angles are not significantly different between WT and TNF-tg mice, indicating minimal experimental variability and similar relative crack extension at the point of instability. *h*) Diagram of a femoral fracture face illustrating the half-notch angle (θ_N; dotted angle), half-crack angle (θ_C; solid angle), region of the notch (N), stable crack growth (S), unstable cracking (U), and the direction of force application (F). Bars represent group means and error bars correspond to standard deviations. Statistically significant differences were determined by unpaired t-tests: * $p < 0.05$, *** $p < 0.001$.

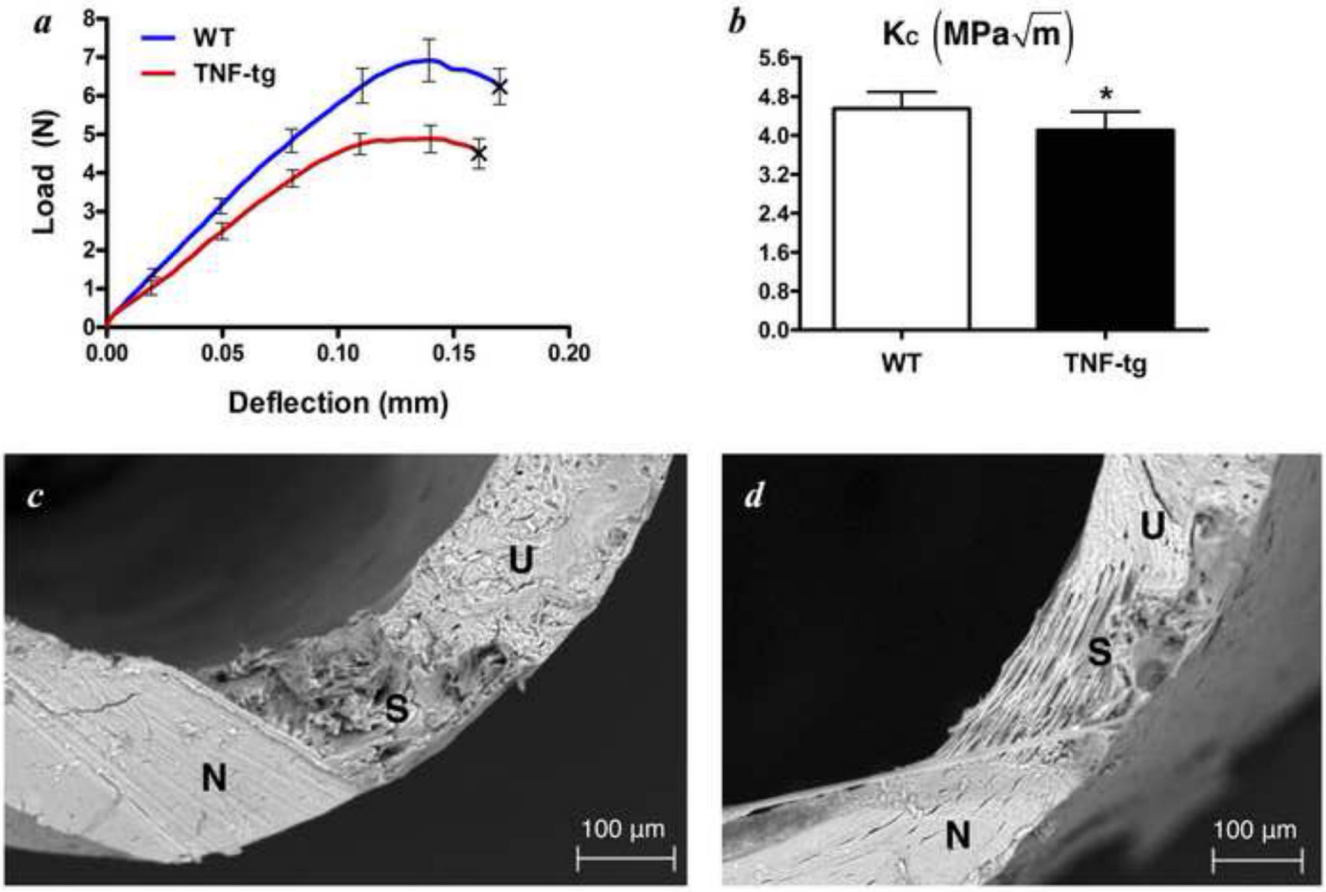

Figure 2. Whole bone femoral fracture toughness is significantly deteriorated in TNF-tg mice compared to WT controls

a) Averaged three point bending load-displacement curves demonstrate a significantly lower fracture load ($p<0.01$) and bending stiffness ($p<0.05$) in the TNF-tg mice (error bars are SEM). *b*) The critical stress intensity factor (K_C; fracture toughness) measured at the point of fracture instability is significantly reduced in TNF-tg mice compared to WT (values are represented as mean and standard deviation). Fracture surfaces from representative WT (*c*) and TNF-tg (*d*) femurs showing the distinct regions of notching (N), stable crack growth (S), and unstable crack growth (U). Statistically significant differences were determined by unpaired t-tests: * $p < 0.05$.

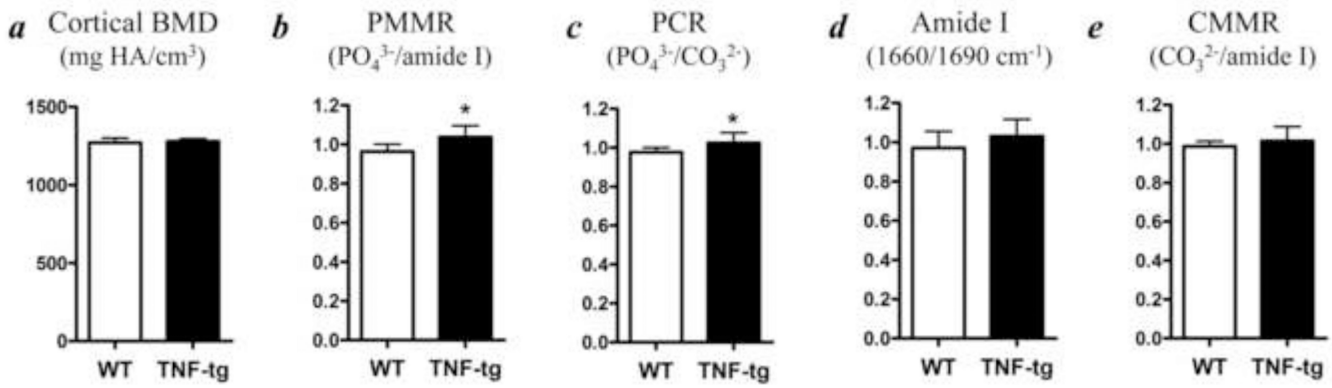

Figure 3. Only minor variations in commonly studied bone compositional metrics exist between WT and TNF-tg mice

a) The cortical bone mineral density measured at the femoral mid-diaphysis is not significantly different, however, the TNF-tg mice have significantly higher phosphate mineral-to-organic matrix (PMMR) ratios (*b*) and phosphate-to-carbonate (PCR) ratios (*c*). The amide I 1660 cm^{-1}/1690 cm^{-1} ratio (*d*) has been described as a measure of 'collagen quality' and has been associated with the relative maturation of enzymatic collagen cross-links in the bone when measured by FTIR. The carbonate mineral-to-matrix ratio (CMMR; *e*) has been hypothesized to indicate increased remodeling of the bone and higher levels have been clinically associated with patients who sustained fractures versus those who did not. No significant differences were found in each of these metrics between the TNF-tg and WT mice. Values are represented as group mean (normalized by the total dataset mean for Raman metrics) and error bars are standard deviation. Statistically significant differences were determined by unpaired t-tests: * $p < 0.05$.

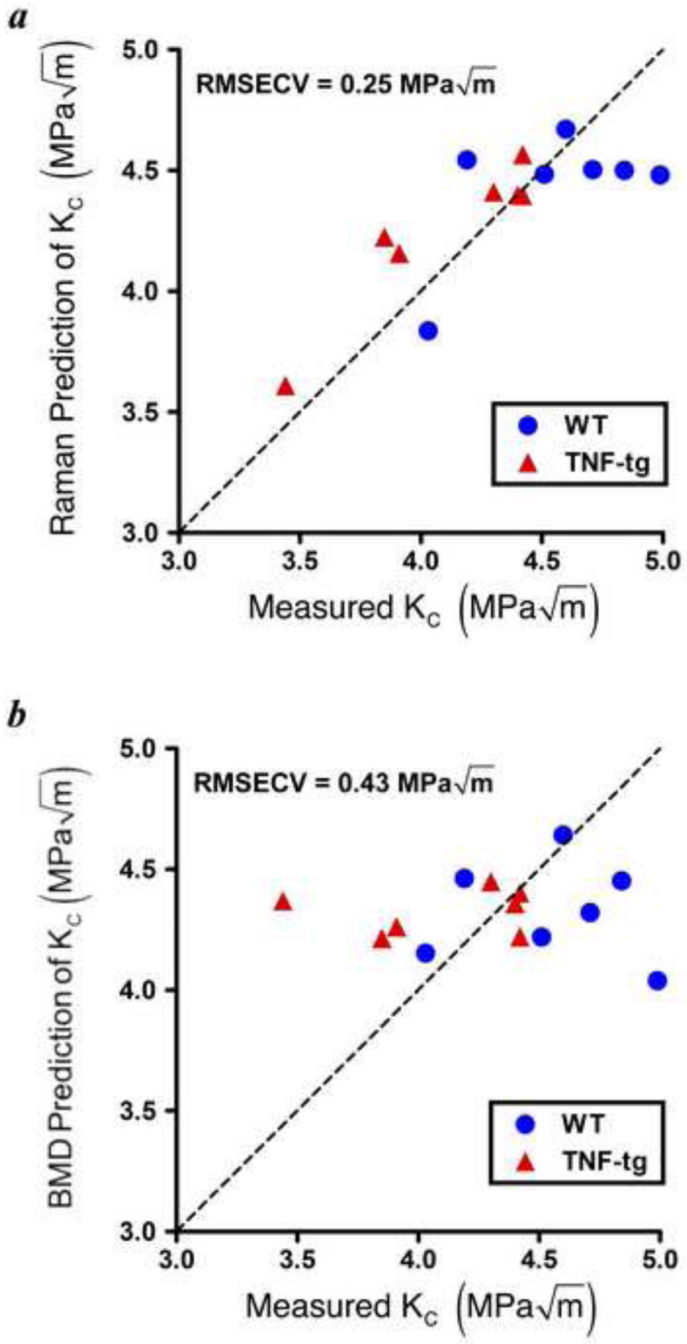

Figure 4. Analysis of the full Raman spectrum through partial-least squares regression (PLSR) provides strong predictions of femoral bone fracture toughness

(*a*) PLSR analysis of the full Raman spectrum gives strong predictions of fracture toughness (K_C) while BMD provides very weak predictions (*b*) as measured by the root mean squared error of cross-validation (RMSECV).

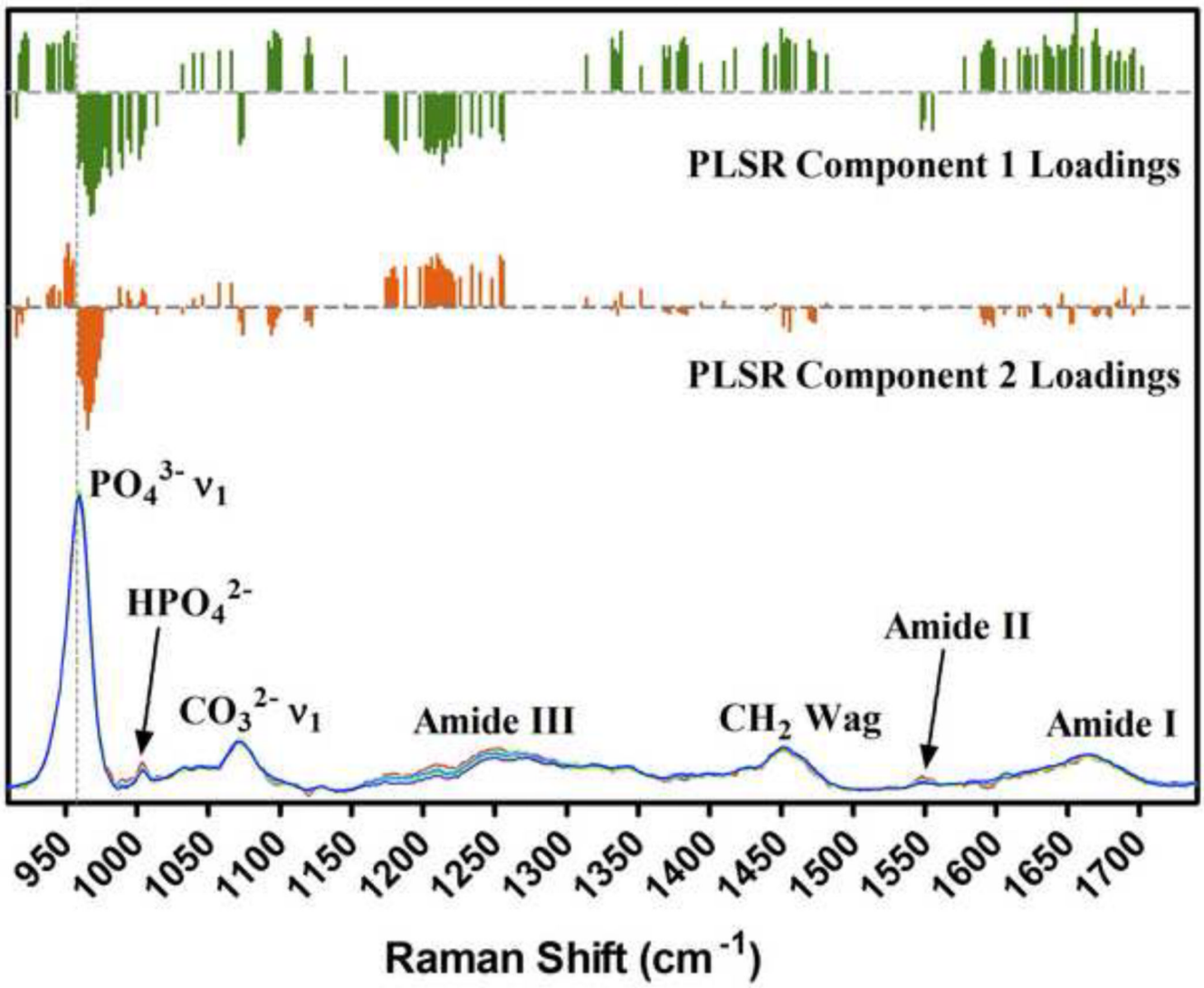

Figure 5. Variations in the phosphate ν_1 peak and organic matrix components are leveraged in the Raman spectrum-based prediction of fracture toughness

PLSR component loadings plotted inline with the Raman spectrum. Loadings correspond to the relative contribution of each wavenumber to the final model from each component. Only wavenumbers with a Variable Importance to Projection Score > 1 are plotted. Analysis of the first (green) and second (orange) component loadings suggests that a shift of the phosphate ν_1 peak (PO_4^{3-} ν_1, 960 cm^{-1}) towards 966 cm^{-1} corresponds with decreased fracture toughness, as evidenced by the predominant 'saw-tooth' features centered at 958 cm^{-1} (vertical dotted line). The first component loading is also leveraged by organic matrix components in the CH_2 and amide I, II, and III regions, which correspond to collagen.

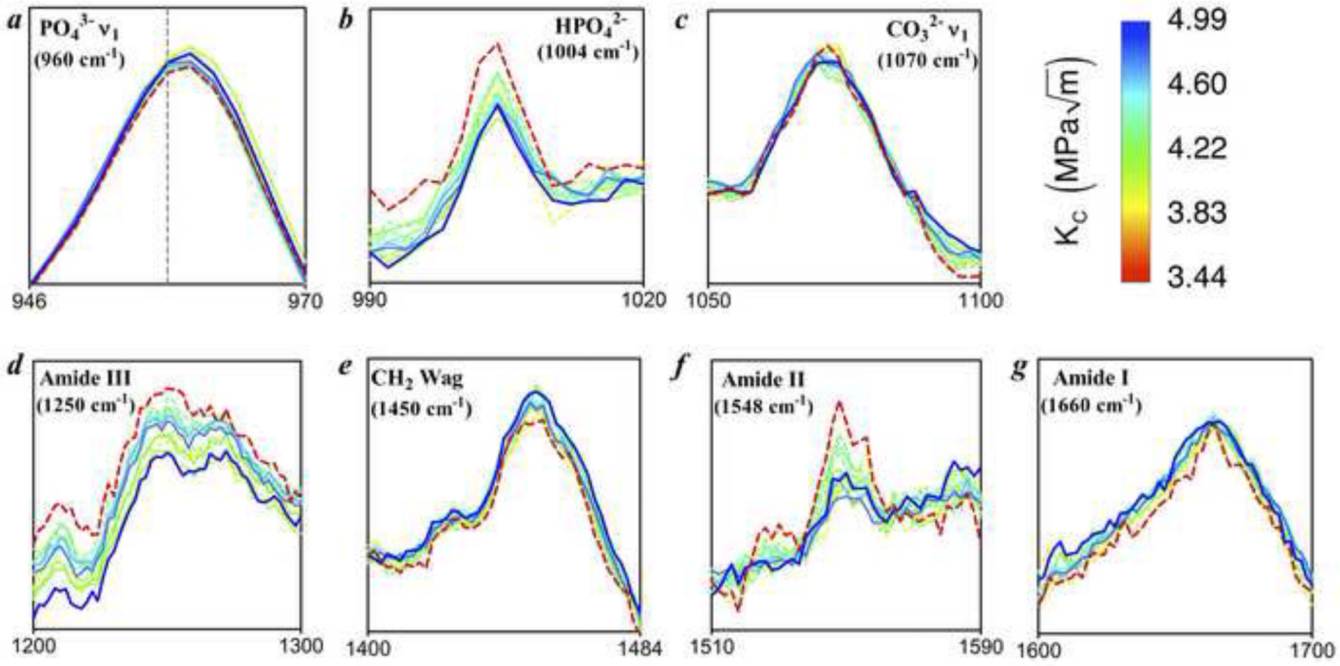

Figure 6. Femoral fracture toughness is associated with the relative intensities of various peaks in the Raman spectrum

Magnified peaks of the Raman spectrum with individual curves colored according to the respective femoral fracture toughness as defined by the color bar. Solid lines correspond to WT specimens and dotted lines correspond to TNF-tg specimens. Plotting the Raman spectra as a function of measured fracture toughness displays differentials that qualitatively reiterate the predictive potential of Raman spectroscopy.

Table 1

Correlations with and predictions of femoral fracture toughness from each predictive variable.

Predictor	R^2 (trend)	
BMD	0.13	0.43
Full Raman Spectrum Prediction	–	0.25
PMMR (PO_4^{3-} υ_1/amide I)	0.70 * (−)	0.26
Crystallinity #	0.60 * (−)	0.28
MR: PMMR + Crystallinity #	0.83 *	0.26
CMMR (CO_3^{2-} υ_1/amide I)	0.37 * (−)	0.37
PO_4^{3-} υ_1 Center of Area	0.35 * (−)	0.40
PCR (PO_4^{3-} υ_1/CO_3^{2-} υ_1)	0.14	0.45
Amide I (1660 cm^{-1}/1690 cm^{-1})	0.05	0.47
Cortical Thickness	0.16	0.43

* Significant correlation with $p < 0.05$.

One outlying data point was left out of the regression based on Cook's distance > 1

MR: Multiple regression of the listed predictors with the R^2 as the adjusted R^2

RMSECV: Root mean squared error of cross-validation